

Structure and Phase Transition Behavior of Sn⁴⁺-Doped TiO₂ Nanoparticles

Yongqiang Cao,[†] Tao He,[‡] Lusong Zhao,[†] Enjun Wang,[†] Wensheng Yang,[§] and Yaan Cao^{*,†}

College of Physics, Nankai University, Tianjin 300071, People's Republic of China, National Center for Nanoscience and Technology, Beijing 100190, People's Republic of China, and College of Chemistry, Jilin University, Changchun 130023, People's Republic of China

Received: July 21, 2009; Revised Manuscript Received: September 14, 2009

Sn⁴⁺-doped TiO₂ nanoparticles have been prepared by sol–gel method and annealed at different temperatures. Doping mode and existing states of Sn⁴⁺ dopants as well as the constituents and phase transition of the resultant nanoparticles have been investigated by X-ray diffraction, X-ray photoelectron spectroscopy, and high resolution transmission electron microscopy techniques. Under a low-temperature annealing (300 °C), the majority of Sn⁴⁺ dopants are connected with Cl[−] ions, forming −Sn−Cl_x at the sample surface, while the others are doped into TiO₂ lattice in substitutional mode. The amount of substitutional Sn⁴⁺ dopants decreases with the increasing annealing temperature. No −Sn−Cl_x is observed at 450 °C. When the annealing temperature is high enough, Sn⁴⁺ ions can replace lattice Ti⁴⁺ ions no matter whether the crystal structure of TiO₂ is anatase or rutile. Furthermore, rutile SnO₂ crystal evolves with the increasing annealing temperature, which can act as seeds for the growth of rutile TiO₂. Accordingly, the phase transition temperature from anatase to rutile of TiO₂ decreases obviously. This may help prepare Sn-doped TiO₂ materials with high photoelectric properties that can be used in many fields, such as photocatalysis and solar cell.

1. Introduction

TiO₂ has attracted extensive attention as a promising material with potential applications in organic contaminant degradation, hydrogen production, photoelectric conversion, and so on.^{1–5} However, TiO₂ is only sensitive to UV light because of its large band gap (3.2 eV). In order to efficiently use solar energy, most of the investigations have been focused on preparing TiO₂ sensitive to visible light during the past several years.^{6–12} Among these, doping TiO₂ with metal ions has been proven to be an effective method. Choi et al.¹³ have reported that doping with Fe, Mo, Ru, Os, Re, V, and Rh in TiO₂ can enhance the photocatalytic activity. Zang and Kisch¹⁴ have claimed that the visible-light response of amorphous TiO₂ modified by various transition metal chlorides can be enhanced greatly. Among all of these dopants, Sn⁴⁺ exhibits great promise. The incorporation of Sn⁴⁺ ions into TiO₂ lattice can effectively suppress the recombination rate of photogenerated charge carriers and increase the redox potential, resulting in the improvement of photocatalytic activity.^{15–17} The doping energy level of Sn⁴⁺ has been determined to be located 0.4 eV below the conduction band of TiO₂.¹⁶ It has been claimed that a random substitution of Sn⁴⁺ for Ti⁴⁺ in rutile phase and some kind of ordering or surface accumulation of Sn⁴⁺ ions for anatase is possible.¹⁷ Moreover, the incorporation of Sn⁴⁺ obviously inhibits the crystallization of anatase nanocrystals.¹⁸ However, so far it is still not clear about the influence mechanism of Sn⁴⁺ doping on the phase structure of TiO₂ during the annealing process as well as the existing states of Sn⁴⁺ ions.

In this work, we have prepared Sn⁴⁺-doped TiO₂ nanoparticles by sol–gel method and annealed them at different temperatures. We have studied the doping mode and existing states of Sn⁴⁺

dopants in TiO₂ during the annealing process and their influence on the temperature of phase transition of TiO₂. Our study can afford a better understanding about the doping mechanism, which may lead to the materials with high photoelectric properties.

2. Experimental Section

2.1. Sample Preparation. Under vigorous stirring, 12 mL of tetrabutyl titanate was added into the mixture of 40 mL anhydrous ethanol and 1 mL deionized water. The pH value of the mixture was 0.5, controlled by adding concentrated HCl (12 M). After stirring for 1.5 h, a 0.6 mL SnCl₄ solution was added dropwise into the mixture. Then, 1 mL of deionized water was added for further hydrolysis. The obtained sol turned into gel under vigorous stirring, which was dried at 100 °C for 12 h and then annealed for 2.5 h at different temperatures (300–700 °C). A series of Sn⁴⁺-doped TiO₂ nanoparticles with the same dopant concentration (13 mol %) were thus obtained. Pure TiO₂ samples were prepared with the same procedures, but without adding SnCl₄. The pure and Sn⁴⁺-doped TiO₂ were designated as P-x and D-x, respectively, where “x” is the annealing temperature.

In all experiments, deionized water ($\rho > 18 \text{ M}\Omega \text{ cm}^{-1}$) was used. All of the chemicals were analytical grade.

2.2. Characterization. X-ray diffraction (XRD) patterns were collected on a Rigaku D/max 2500 X-ray diffractometer (Cu K α , $\lambda = 1.54056 \text{ \AA}$) in the range of 20–80°. X-ray photoelectron spectroscopy (XPS) measurements were carried out with an ESCA Lab 220i-XL spectrometer (Al K α , 1486.6 eV). The XPS spectra were calibrated with respect to the binding energy of the adventitious C1s peak at 284.8 eV and were deconvoluted using XPSPEAK software. Transmission electron microscopy (TEM) and high resolution TEM (HRTEM) analysis were conducted using a JEOL 3010, for which the samples were prepared by applying a drop of ethanol suspension onto an amorphous carbon-coated copper grid and dried naturally.

* Corresponding author. Phone: +86-22-66229598. E-mail: caoyaan@yahoo.com.

[†] Nankai University.

[‡] National Center for Nanoscience and Technology.

[§] Jilin University.

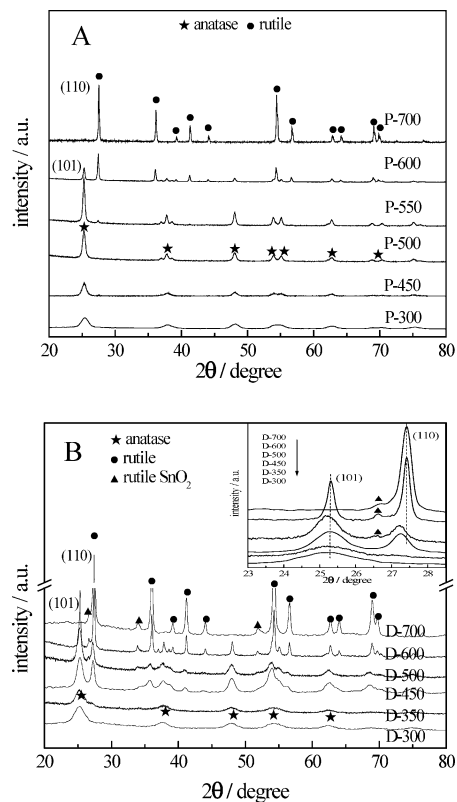


Figure 1. XRD patterns of (A) pure TiO₂ and (B) Sn⁴⁺-doped TiO₂ samples. Inset of (B) displays an expanded view of the spectra ranging from 23 to 28.5°.

3. Results and Discussion

3.1. Phase Transition of Sn⁴⁺-Doped TiO₂. Figure 1A shows the XRD spectra of pure TiO₂ samples annealed at temperatures ranging from 300 to 700 °C. It can be observed readily that P-300, P-450, and P-500 samples exhibit an anatase structure.¹⁹ A weak peak at around 27.3° is found in P-550 besides the anatase peaks, indicating the presence of a small amount of rutile structure in the sample. Compared with P-550, the diffraction peaks of rutile in P-600 sample increase as those of anatase decrease, which means the phase transition from anatase to rutile in the sample occurs. A pure rutile structure is observed in P-700 sample, implying the anatase structure is completely transformed into rutile. Thus, the lowest temperature of phase transition from anatase to rutile is around 550 °C for pure TiO₂, which is lower than that for the bulk material (>600 °C) because of the nanosize effects.

The XRD spectra of Sn⁴⁺-doped TiO₂ samples annealed at temperatures ranging from 300 to 700 °C are demonstrated in Figure 1B. D-300 sample shows only an anatase structure. The main structure of D-350 sample is still anatase, while a weak peak appears at around 27.3°, suggesting the formation of rutile TiO₂. Hence, the lowest phase transition from anatase to rutile can take place at around 350 °C for Sn⁴⁺-doped TiO₂ samples, which is about 200 °C lower than that for pure TiO₂ (550 °C).

Besides the diffraction peaks for anatase and rutile TiO₂, two weak peaks are observed at around 33.95° and 51.92° in D-450 sample, indicating a small amount of rutile SnO₂ is formed (Figure 1B).²⁰ For Sn⁴⁺-doped TiO₂ samples, the peak intensities for rutile TiO₂ and rutile SnO₂ increase gradually as the annealing temperature increasing from 450 to 600 °C (curves D-450 ~ D-600). For D-700 sample, only rutile TiO₂ and SnO₂ can be observed. Furthermore, with the increase of annealing temperature, the diffraction peaks of anatase and rutile TiO₂

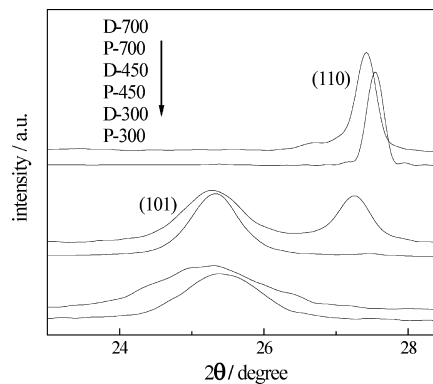


Figure 2. Spectra from Figure 1, showing an expanded view of XRD patterns of rutile (110) and anatase (101) for pure and Sn⁴⁺-doped TiO₂ samples annealed at 300, 450, and 700 °C.

are gradually narrowed, and the peak positions shift gradually to the same values as those for pure TiO₂, accompanying with the increase of the amount of rutile SnO₂ (inset of Figure 1B). This implies that Sn⁴⁺ dopants in TiO₂ changes gradually from doping state to rutile SnO₂ during the phase change from anatase to rutile, and the Sn⁴⁺ ions doped in TiO₂ can promote the formation of rutile TiO₂, which is further discussed in the following parts. In addition, the observed narrowing of peak width is caused by several factors, such as the increase in the particle size, the decrease in the difference in strain in different grains, and the decrease in the lattice defects.

3.2. Doping Mode and Existing States of Sn⁴⁺ Ions in TiO₂.

3.2.1. XRD. It can be seen from Figure 1 that the diffraction peaks shift to smaller angles for all Sn⁴⁺-doped TiO₂ samples than those for pure TiO₂. This trend can be seen much clearer in Figure 2, which is an expanded view of XRD patterns related to (101) and (110) planes for pure and Sn⁴⁺-doped TiO₂ samples annealed at 300, 450, and 700 °C, respectively. If the electronegativity and ionic radius of the doping metal ions match those of the lattice metal ions in the oxide, the lattice metal can be substituted by the doping ions during the sample preparation process.²¹ Because the electronegativity and ionic radius of Sn⁴⁺ ion (1.8, 69 pm) are close to those of Ti⁴⁺ ion (1.5, 53 pm),¹⁶ it is expected that Sn⁴⁺ ions can replace lattice Ti⁴⁺ ions in TiO₂ and, accordingly, occupy the lattice Ti⁴⁺ positions. Since the ionic radius of Sn⁴⁺ is slightly larger than that of lattice Ti⁴⁺, the lattice parameters, cell volume, and *d* values of TiO₂ increases after doping. Indeed, these are confirmed by our experimental results (Table 1). Accordingly, the peak positions of all Sn⁴⁺-doped TiO₂ shift to lower diffraction angles.²² This also indicates that Sn⁴⁺ ions can be doped into TiO₂ in substitutional mode no matter whether the structure of TiO₂ is anatase or rutile. In comparison with pure TiO₂, moreover, the decrease in crystal size of Sn⁴⁺-doped TiO₂ samples (Table 1) is attributed to the Sn⁴⁺ ions doping, which can suppress the growth of anatase and rutile grains because of the dissimilar boundaries.^{15,18,24,25} It is also noted that the particle size increases with the increasing annealing temperature for the same type of nanoparticles (Table 1). This is because annealing can enhance the diffusion at the interface and inside the particle and lead to particle agglomeration. The disappearance of grain boundary and the coalescence of particle clusters into single crystalline lattices will eventually take place so as to minimize the surface free energy, resulting in the coarsening of nanoparticles.

3.2.2. XPS Analysis. XPS analysis has been performed to further study the existing states of Sn⁴⁺ ions in TiO₂. Figure 3 shows the Sn3d XPS spectra of D-300, D-450, and D-700 samples, respectively. The binding energy and full width at half-

TABLE 1: Crystalline Size, $d_{(hkl)}$ Value, Cell Parameter, and Cell Volume for Pure and Doped Samples Annealed at 300, 450, and 700 °C, Which Were Calculated According to the Literature^{15,23}

sample	crystallite size (nm)			cell parameters (Å)				
	anatase	rutile	$d_{(hkl)}$ value (Å)	anatase	rutile	cell vol (Å ³)		
P-300	6.76		$d_{(101)A} = 3.503$	$a = b = 3.7820$	$c = 9.3100$	133.17		
D-300	4.65		$d_{(101)A} = 3.533$	$a = b = 3.7971$	$c = 9.6920$	139.74		
P-450	10.83		$d_{(101)A} = 3.517$	$a = b = 3.7846$	$c = 9.5283$	136.48		
D-450	8.42	16.04	$d_{(101)A} = 3.523$	$a = b = 3.7921$	$c = 9.5260$	136.98		
P-700		63.48	$d_{(110)R} = 3.237$			$a = b = 4.5777$	$c = 2.9573$	61.97
D-700		37.16	$d_{(110)R} = 3.250$			$a = b = 4.5963$	$c = 2.9611$	62.56

TABLE 2: Binding Energy (BE) and fwhm of Sn Species in D-300, D-450, and D-700 Samples

sample	Sn ⁴⁺ dopant		−Sn−Cl _x		SnO ₂ + SnO _x ($x < 2$)	
	Sn3d _{5/2}	Sn3d _{3/2}	Sn3d _{5/2}	Sn3d _{3/2}	Sn3d _{5/2}	Sn3d _{3/2}
D-300 BE	485.4	494.3	487.0	495.5		
fwhm	2.65	2.65	2.36	2.64		
D-450 BE	485.3	494.2			486.2	494.8
fwhm	2.65	2.65			2.30	2.27
D-700 BE	485.3	494.2			486.4	495.0
fwhm	2.65	2.65			2.30	2.48

maximum (fwhm) of Sn species in Sn⁴⁺-doped TiO₂ samples are listed in Table 2.

The doublet peak (485.4 and 494.3 eV) in the Sn3d XPS spectrum of D-300 sample (Figure 3a) is ascribed to Sn3d_{5/2} and Sn3d_{3/2} of the substitutional Sn⁴⁺ dopants in the lattice, since the peak position of Sn3d_{5/2} (485.4 eV) is located between that of SnO₂ (486.6 eV) and metallic Sn (484.6 eV).²⁶ The strong doublet peak at 487.0 and 495.5 eV in Figure 3a is attributed to Sn3d_{5/2} and Sn3d_{3/2} of Sn⁴⁺ ions that are connected with surface Cl ions, present in the form of −Sn−Cl_x on the sample surface. The formation of a chemical bond between Sn⁴⁺ and Cl[−] ions is easier than that between Ti⁴⁺ and Cl[−] ions during the reaction because the electronegativity of Sn (1.8) is larger than that of Ti (1.5).¹⁶ It is also believed that Cl[−] ion cannot replace lattice O and occupy its position during the preparation because the ionic radius of Cl[−] ion is much larger (1.81 Å) than that of O^{2−} ion (1.40 Å).²⁷ Our XPS result indicates the presence of Cl species in D-300 sample (inset of Figure 3a). Because there is no XRD signal observed from SnO₂ in D-300 (Figure 1) and it has been reported that Cl species can exist on the sample surface,²⁸ it is suggested that Cl[−] ions are connected with Sn⁴⁺ sites, resulting in the formation of −Sn−Cl_x on the surface of D-300.

The doublet peak (485.3 and 494.2 eV) in Figure 3b,c is ascribed to Sn3d_{5/2} and Sn3d_{3/2} of the substitutionally doped Sn⁴⁺ ions in D-450 and D-700 samples, respectively. The peak attributed to −Sn−Cl_x species disappears when the annealing

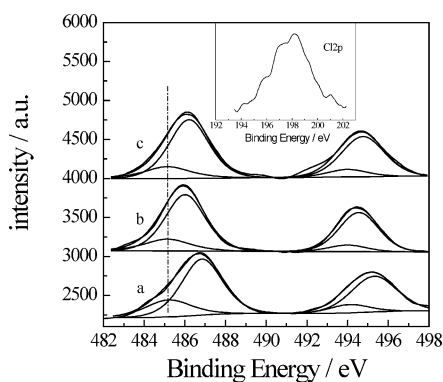


Figure 3. Sn3d XPS spectra of (a) D-300, (b) D-450, and (c) D-700. Inset is the Cl2p XPS spectrum of D-300.

temperature is at 450 °C and higher, implying they are changed into new Sn species. Meanwhile, a new doublet peak can be observed at 486.2 and 494.8 eV after deconvolution for the sample annealed at 450 °C and at 486.4 and 495.0 eV for 700 °C. This newly formed peak is ascribed to tin oxide, a mixture of SnO₂ and SnO_x ($x < 2$), since the Sn3d_{5/2} binding energy for pure SnO₂ is 486.6 eV and no Cl XPS signal is observed in these samples. The increase of binding energy for tin oxide with the annealing temperature indicates there is an increase of the amount of SnO₂ and a decrease of SnO_x with the increasing annealing temperature. This is consistent with the aforementioned XRD results. The tin oxide comes mainly from the surface −Sn−Cl_x as well as from some substitutional Sn⁴⁺ dopants, which will be thoroughly discussed below.

3.2.3. TEM and HRTEM. Figure 4 shows the TEM images of P-450 and D-450 samples, respectively. Nanoparticles with a diameter of about 10 nm are observed in both samples. The electron diffraction (ED) patterns of the selected area on D-450 sample (inset of Figure 4b) shows the strong Debye–Scherrer rings and complicated bright spots, indicating the coexistence of polycrystalline anatase and rutile crystallites.^{29,30} This agrees with the aforementioned conclusion that the Sn⁴⁺ ions doped in TiO₂ can promote the formation of rutile TiO₂. Figure 5 displays the HRTEM images of P-450 and D-450 samples, respectively. For anatase structure, the fringe spacing (d) of (101) crystallographic plane is determined to be 3.55 Å for D-450 sample (Figure 5b) and 3.52 Å for P-450 sample (Figure 5a). This implies that Sn⁴⁺ ions are doped into TiO₂ lattice in substitutional mode in D-450 sample since the ionic radius of Sn⁴⁺ (69 pm) is larger than that of the lattice Ti⁴⁺ (53 pm).¹⁶ Furthermore, a fringe spacing of 3.22 and 3.38 Å corresponding to the (110) planes of both rutile TiO₂ and rutile SnO₂ are observed in D-450 sample, respectively (Figure 5c,d). All of these are consistent with the aforementioned XRD results.

3.3. Mechanism of the Formation of Tin Oxide and Rutile TiO₂ in Sn⁴⁺-Doped TiO₂. Sn⁴⁺-doped TiO₂ samples were prepared by the prehydrolysis of tetrabutyl titanate at room temperature, as described in Experimental Section. When annealed at 300 °C, some Sn⁴⁺ ions were doped into TiO₂ lattice in substitutional mode, while most of them formed into

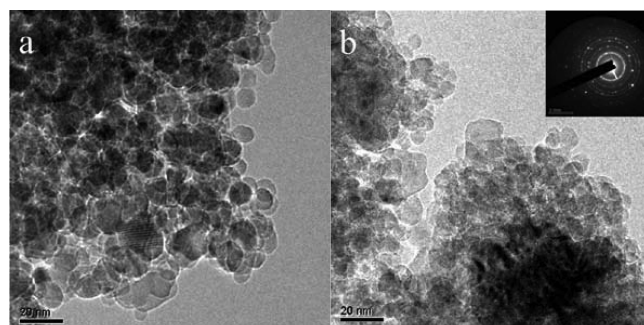


Figure 4. TEM images of (a) P-450 and (b) D-450 samples.

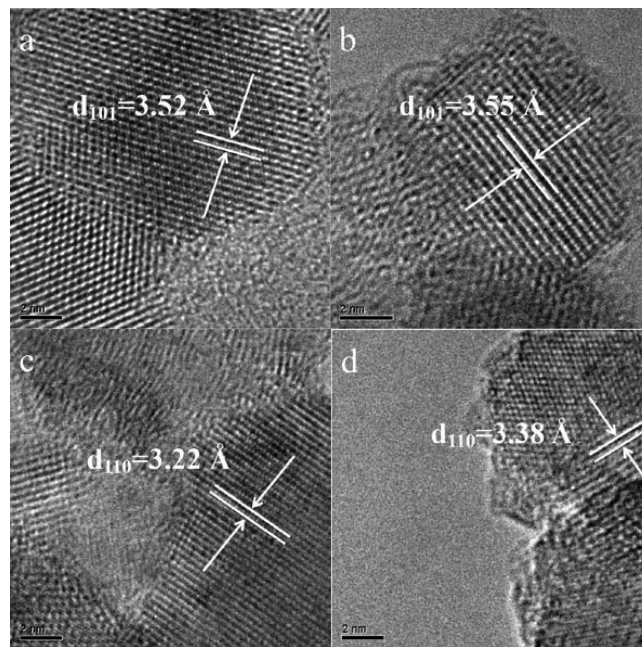


Figure 5. HRTEM images of (a) P-450 and (b–d) D-450 samples.

—Sn—Cl_x species at the sample surface. When annealed at 450 °C, the surface —Sn—Cl_x species could react with O₂ to form tin oxide. Thus, no —Sn—Cl_x signal was observed. Meanwhile, the lattice vibration of Sn⁴⁺-doped TiO₂ sample was enhanced. The doped Sn⁴⁺ ions could gain enough energy and escape from the bondage of lattice. The higher the annealing temperature, the easier the Sn⁴⁺ ions could escape from the lattice. The escaped Sn⁴⁺ could react with O²⁻ to form tin oxide too. This can explain why the amount of substitutional Sn⁴⁺ dopants decreased in both D-450 and D-700 samples and the amount of tin oxide increased with increasing annealing temperature. If the amount of oxygen is not high enough during annealing, the annealing time is not long enough, and/or the annealing temperature is not high enough, the tin oxide will be composed of rutile SnO₂ and SnO_x ($x < 2$). The higher the annealing temperature, the more the amount of rutile SnO₂ is. The rutile SnO₂ crystal could further induce the nucleation and growth of rutile TiO₂,¹⁸ leading to an obvious decrease in the temperature of phase transition from anatase to rutile of TiO₂.

4. Conclusions

In this work, we found that Sn⁴⁺ ions can be doped into TiO₂ lattice in substitutional mode and/or exist in the form of —Sn—Cl_x or tin oxide, which depends on the annealing temperature. The rutile SnO₂ crystal can act as seeds for the growth of rutile TiO₂, resulting in a lower phase-transition temperature from anatase to rutile of TiO₂. Hopefully, this may afford a better

understanding about the doping mechanism, leading to the preparation of materials with high photoelectric properties that can be used in many fields, such as photocatalysis, photosynthesis, and solar cell.

Acknowledgment. This work was supported by National Natural Science Foundation of China (No. 50872056). T.H. thanks the Hundred-Talent Program of Chinese Academy of Sciences.

References and Notes

- (1) Hoffmann, M. R.; Martin, S. T.; Choi, W.; Bahnemann, D. W. *Chem. Rev.* **1995**, *95*, 69.
- (2) Linsebigler, A. L.; Lu, G.; Yates, J. T. *J. Chem. Rev.* **1995**, *95*, 735.
- (3) Thompson, T. L.; Yates, J. T. *J. Chem. Rev.* **2006**, *106*, 4428.
- (4) Chen, X.; Mao, S. S. *Chem. Rev.* **2007**, *107*, 2891.
- (5) Hagfeldt, A.; Grätzel, M. *Chem. Rev.* **1995**, *95*, 49.
- (6) Dawson, A.; Kamat, P. V. *J. Phys. Chem. B* **2001**, *105*, 960.
- (7) Asahi, R.; Morikawa, T.; Ohwaki, T.; Aoki, K.; Taga, Y. *Science* **2001**, *293*, 269.
- (8) Sakthivel, S.; Kisch, H. *Angew. Chem., Int. Ed.* **2003**, *42*, 4908.
- (9) Macyk, W.; Kisch, H. *Chem.—Eur. J.* **2001**, *7*, 1862.
- (10) Borgarello, E.; Kiwi, J.; Grätzl, M.; Pelizzetti, E.; Visca, M. *J. Am. Chem. Soc.* **1982**, *104*, 2996.
- (11) Duonghong, D.; Borgarello, E.; Grätzl, M. *J. Am. Chem. Soc.* **1981**, *103*, 4685.
- (12) O'Regan, B.; Grätzel, M. *Nature* **1991**, *353*, 737.
- (13) Choi, W.; Termin, A.; Hoffmann, M. R. *J. Phys. Chem.* **1994**, *98*, 13669.
- (14) Zang, L.; Macyk, W.; Lange, C.; Maier, W. F.; Antonius, C.; Meissner, D.; Kisch, H. *Chem.—Eur. J.* **2000**, *6*, 379.
- (15) Lin, J.; Yu, J. C.; Lo, D.; Lam, S. K. *J. Catal.* **1999**, *183*, 368.
- (16) Cao, Y.; Yang, W.; Zhang, W.; Liu, G.; Yue, P. *New J. Chem.* **2004**, *28*, 218.
- (17) Fresno, F.; Tudela, D.; Coronado, J. M.; Garcia, M. F.; Hungria, A. B.; Soria, J. *Phys. Chem. Chem. Phys.* **2006**, *8*, 2421.
- (18) Yu, J.; Liu, S.; Zhou, M. *J. Phys. Chem. C* **2008**, *112*, 2050.
- (19) Liu, H.; Yang, W.; Ma, Y.; Cao, Y.; Yao, J. *New J. Chem.* **2002**, *26*, 975.
- (20) Fresno, F.; Coronado, J. M.; Tudela, D.; Soria, J. *Appl. Catal., B* **2005**, *55*, 159.
- (21) Xu, Y. L. *The Basics of Semiconducting Oxides and Compounds*; Press of Xi'an Electronic Science and Technology University: Xi'an, 1991.
- (22) Kitano, M.; Funatsu, K.; Matsuoaka, M.; Ueshima, M.; Anpo, M. *J. Phys. Chem. B* **2006**, *110*, 25266.
- (23) Yu, J. C.; Lin, J.; Kwok, R. W. M. *J. Phys. Chem. B* **1998**, *102*, 5094.
- (24) Cong, Y.; Zhang, J.; Chen, F.; Anpo, M. *J. Phys. Chem. C* **2007**, *111*, 6976.
- (25) Huang, Y.; Zheng, Z.; Ai, Z.; Zhang, L.; Fan, X.; Zou, Z. *J. Phys. Chem. B* **2006**, *110*, 19323.
- (26) Wang, J.; Wu, W.; Feng, D. *The introduction of electronic spectroscopy*; The Publishing House of Defense Industry: Beijing, 1992.
- (27) Sun, Z. *The Structural Chemistry*; Press of Shaanxi Normal University: Xi'an, 1990.
- (28) Zhu, J.; Zheng, W.; He, B.; Zhang, J.; Anpo, M. *J. Mol. Catal. A* **2004**, *216*, 35.
- (29) Zhao, L.; Han, M.; Lian, J. *Thin Solid Films* **2008**, *516*, 3394.
- (30) Chang, J. A.; Vithal, M.; Baek, I. C.; Seok, S. I. *J. Solid State Chem.* **2009**, *182*, 749.

JP9069288